

Field propagation of a metallic grid slab that acts as a metamaterial

Chao-Hsi Tsao*, Jyh-Long Chern

Department of Photonics, Institute of Electro-Optical Engineering, Microelectronics and Information System Research Center, National Chiao Tung University, Hsinchu 300, Taiwan

Received 6 September 2005; received in revised form 14 December 2005; accepted 23 December 2005

Available online 6 January 2006

Communicated by A.R. Bishop

Abstract

A metallic grid slab has been shown to work as a novel metamaterial which can shape the divergent field emitted from an embedded monopole microwave antenna into a directive transmission at a specific frequency. The transmission of such subwavelength slab remains an issue of challenge. In this work, we experimentally investigate the transmitted behavior of such subwavelength grid slab to explore the underlying mechanism of wave propagation. It is found that there is a large tolerance of directive emission even with a tilted slab. The deviation along the directive emission direction is analyzed based on the interference theory.

© 2005 Elsevier B.V. All rights reserved.

Keywords: Metamaterials; Left-handed materials; Directive emission

1. Introduction

The original work of left-handed metamaterials (LHM) can be traced back to Veselago who explored the consequence of the simultaneous occurrence of negative permeability and permittivity [1]. Since his work in 1968, left-handed metamaterials have attracted lot of interests. Substantial progress has been made, mainly because of the works of Pendry et al., and other research groups [2–8]. A combination of simultaneously negative ϵ and μ can cause many intriguing properties such as negative Goos–Hänchen shift [9], reversed circular Bragg phenomenon [10], photon helicity reversal [11] and unusual quantum optical effects [12]. One of the most remarkable applications of LHMs is perfect lens [13]. Until recently many experiments were performed to test this as a theoretical hypothesis, and a large number of successful reports were contributed [2–8] to prove the existence of metamaterials with a negative index of refraction. In 2000, Pendry proposed a superlens of negative index refraction in order to break diffraction limits under certain conditions [13]. After that, not only an experimental demonstra-

tion of this superlens in microwave range was published [14] but also other forms, different from a split ring resonator (SRR), were also demonstrated [15,16]. In order to understand the optical properties of the LHM slab, the finite difference in time domain (FDTD) method is often used to numerically emulate the propagation phenomenon. For example, Loschialpo et al. reported the FDTD snapshots of the magnitude of the electromagnetic field propagating from a divergent source [17]. These works also have helped to stimulate the general interest of metamaterials in the community.

Not only structures with a negative refractive index attract a lot of attention, metamaterials with an effective index of refraction between 0 and 1 draw many interests as well, even though they are not as popular as LHMs in the literatures. Enoch et al., working in the microwave domain, proposed a metallic composite material which allowed an embedded monopole electromagnetic wave source to have its emission field limited in a narrow angular distribution, called directive emission [18]. Their experiment showed that a metallic grid slab acts as a metamaterial with an effective refractive index less than unity. That directive emission is quiet interesting and is understood intuitively on the basis of Snell's law with the refractive index less than 1.

Instead of a follow-up of the study, we focus on investigating the propagating behavior of electromagnetic wave through

* Corresponding author.

E-mail addresses: chaohsi.eo92g@nctu.edu.tw (C.-H. Tsao), jlchern@faculty.nctu.edu.tw (J.-L. Chern).

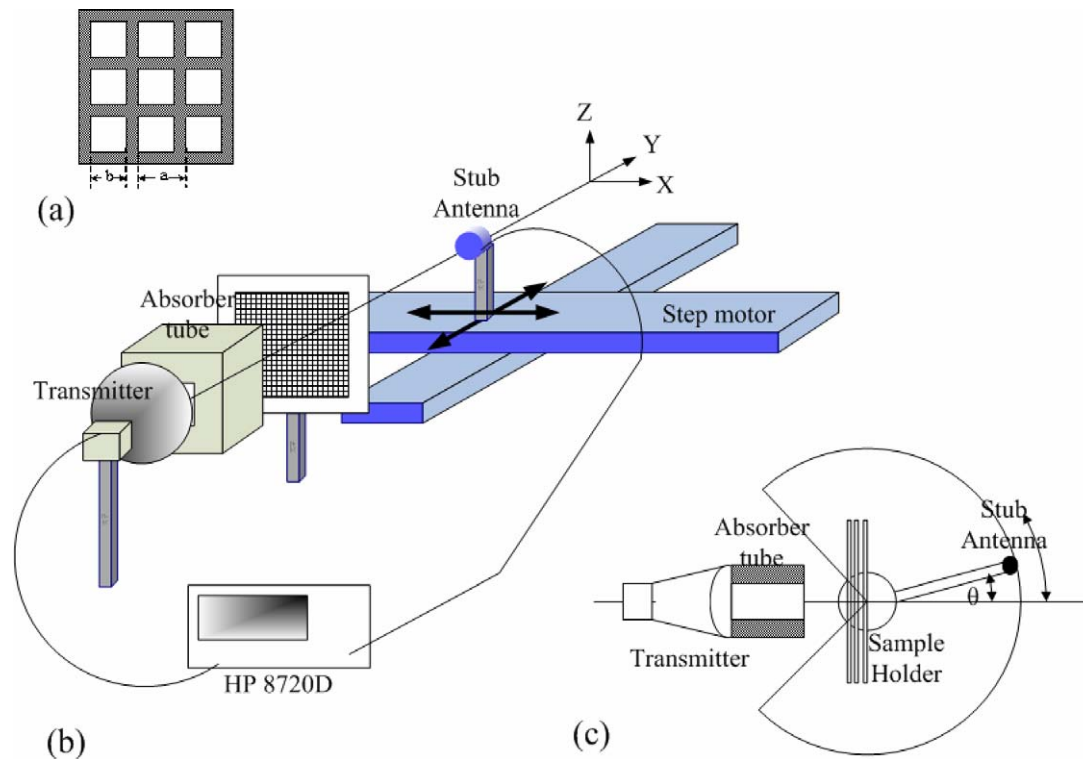


Fig. 1. (a) The schematic diagram of a metallic grid where $a = 5.8$ mm and $b = 4.85$ mm, and the distance between slabs is 6.8 mm (not shown in the diagram). (b) The layout of the experimental setup. This configuration uses 2 linear step motors to analyze the two-dimensional electric field distribution. (c) The alternative configuration is designed for measuring the angular distribution of the electric field.

such subwavelength metallic grid slab. In this Letter, we use a composite metallic grid slab as our sample to experimentally explore these novel features. Experiments are carried out using microwave beams, allowing us to deduce extensive results due to the different incident aspects. These results may provide a possible explanation and help us to understand the mechanism of the interaction between the incident microwave and the metallic pattern. The methodology we manipulated in this Letter is replacing the embedded monopole source by a collimated external transmitter owing to the intention of observation of propagating path of the passing electromagnetic beams. The main purpose is not to demonstrate directive emission but to explore the way that electromagnetic beam propagates and the underlying mechanism. A simple and effective model will be provided in this Letter to explain how the electromagnetic beam travels inside the medium on the basis of interference principle. The Letter is organized as follows: in Section 2, the characteristics of the sample and measurement method are summarized, while in Section 3 we presented the experimental results. Final section is the conclusion.

2. Materials and experimental method

The metamaterial is composed of copper grids made by using the conventional printed circuits technology of electronics and the thickness of copper slice is about 0.1 mm, then is coated on the printed circuit board (PCB) whose thickness is 1 mm. Six identical grids with a square lattice whose pitch is 5.85 mm comprise the structure of sample with the separating

distance, $d = 5.88$ mm, and the opening square of each unit cell is $4.9 \text{ mm} \times 4.9 \text{ mm}$, as shown in Fig. 1(a). An Agilent vector network analyzer (VNA), HP8720D (frequency range 0.05–20.05 GHz), is utilized for the transmission spectrum analysis and the spatial electric field measurements. A lens-horn antenna (FLANN 16810-FA) driven by the VNA is used to produce the z directional linearly polarized microwave, propagating along the y direction. A tiny radio frequency (RF) stub antenna (HERLEY 845CX-10) is regarded as the microwave receiver to analyze the detailed spatial field distribution. The physical size of the detecting area of this stub antenna is around $1 \text{ cm} \times 1 \text{ cm}$ and it works well within the experimental frequencies region (10 to 17 GHz). The sample holder is capable of rotation driven by a rotary motor and its movements can be controlled by a personal computer. In order to prevent the noise reflected from the environments, a microwave absorber is used to surround the entire experimental system. The detailed schematic diagrams of experimental layout are shown in Fig. 1(b) and (c).

Despite taking a lens-horn antenna as the microwave transmitter, the produced electromagnetic field disperses with the propagating distance through free space due to its nature. In order to ensure that the incident electromagnetic wave acts as a collimated beam when penetrating through the metamaterial, the sample is not allowed to be placed too far away from the transmitter. The function of the rectangular tube made of microwave absorbing material is helpful to filter off the outer region of the produced microwave which is originally emitted by a larger angle. The opening of the tube is about $7.5 \text{ cm} \times 7.5 \text{ cm}$ and its length is 20 cm. The resultant propagating electromag-

netic field in free space is shown in the top left corner of Fig. 4, in which, the dash box shows the location of the sample, and the y -axis indicates the distance from the exit window of the confinement tube.

3. Experimental results

In the realization of the metallic mesh, many theoretical and experimental works have already disclosed that the continuous thin wires are characterized by plasma frequency [7,19,20], the equivalent permittivity of which is governed by a plasma frequency in the microwave domain: $\epsilon_{\text{eff}} = 1 - \omega_p^2/\omega^2$, where ω_p is the plasma frequency and ω is the working frequency of the electromagnetic wave. If the frequency of the electromagnetic wave is chosen to be a little larger than the plasma frequency, then the optical index is positive and less than one, and eventually very close to zero [18].

Pendry et al. proposed a mechanism with periodic structures built of very thin wires to depress the plasma frequency into GHz band [6]. Consider the metallic grid slab as a periodic thin wire structure, the depressed plasma frequency can be realized by the concepts of dilution of the average concentration of electrons and enhancement of the effective electron mass through self-inductance. Despite the suppression of the vertical wires, the analogy from the metallic grid slab to periodic thin wires is still meaningful. The z directional polarized electromagnetic wave implies that the interaction between the electric field and the vertical wires is negligible. The depressed plasma frequency for periodic wires can be deduced by the effective density of electrons, n_{eff} , and the effective electron mass, m_{eff} , or by the lattice constant, a , and the radius of the thin wire, r , as follows,

$$\omega_p^2 = \frac{n_{\text{eff}} e^2}{\epsilon_0 m_{\text{eff}}} = \frac{2\pi c^2}{a^2 \ln(a/r)}, \quad (1)$$

where e is the charge of electron, c is the light speed in vacuum and ϵ_0 is the permittivity of vacuum.

Eq. (1) is derived from the case of cylindrical symmetric wire, but however, for the metamaterial used in our experiment, the copper grid is composed of rectangular sheets instead of wires. To roughly estimate the depressed plasma frequency, we substitute the estimated effective radius of the wire which is defined as follows into Eq. (1):

$$r_{\text{eff}} = \sqrt{\frac{W \times H}{\pi}} = \sqrt{\frac{(9.5 \times 10^{-4}) \times (1 \times 10^{-4})}{\pi}} \approx 1.74 \times 10^{-4} \text{ (m)}, \quad (2)$$

where W and H are the line width and metal thickness of copper grids, respectively. Hence, the plasma frequency of the metallic grid slab can be calculated by

$$\omega_p^2 = \frac{2\pi(3 \times 10^8)^2}{(5.85 \times 10^{-3})^2 \times \ln(5.85 \times 10^{-3}/1.74 \times 10^{-4})} \approx (10.9 \text{ GHz})^2. \quad (3)$$

A transmission spectrum, as shown in Fig. 2, is measured with the normal incidence in order to experimentally find the plasma frequency of our sample. The incident electromagnetic waves with frequencies lower than 11 GHz were nearly completely suppressed when the metamaterial is composed of six layers. It should be emphasized that even a lower equivalent permittivity can be obtained if the working frequency was chosen closer to the plasma frequency, a higher reflection will occur when the incident angle is large. For the compromise between low equivalent refractive index and high transmission power, we chose 13 GHz as our working frequency for the following experiments. Fig. 3 summarizes the comparison of the two-dimensional fields of electromagnetic beam with incident

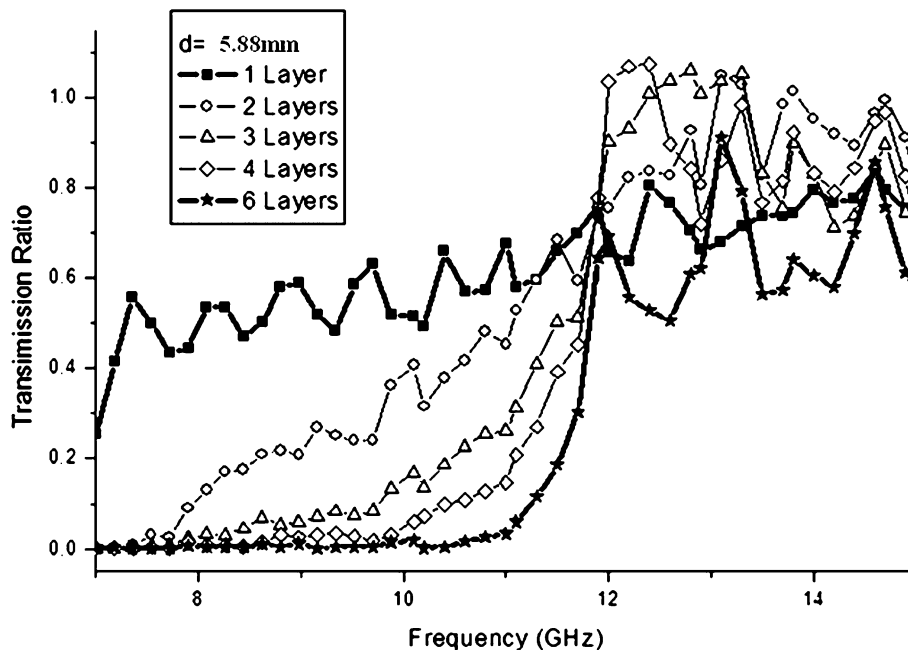


Fig. 2. The transmission spectra from 7 to 15 GHz with the number of metallic grid slabs, n , namely n is from 1 to 6, respectively.

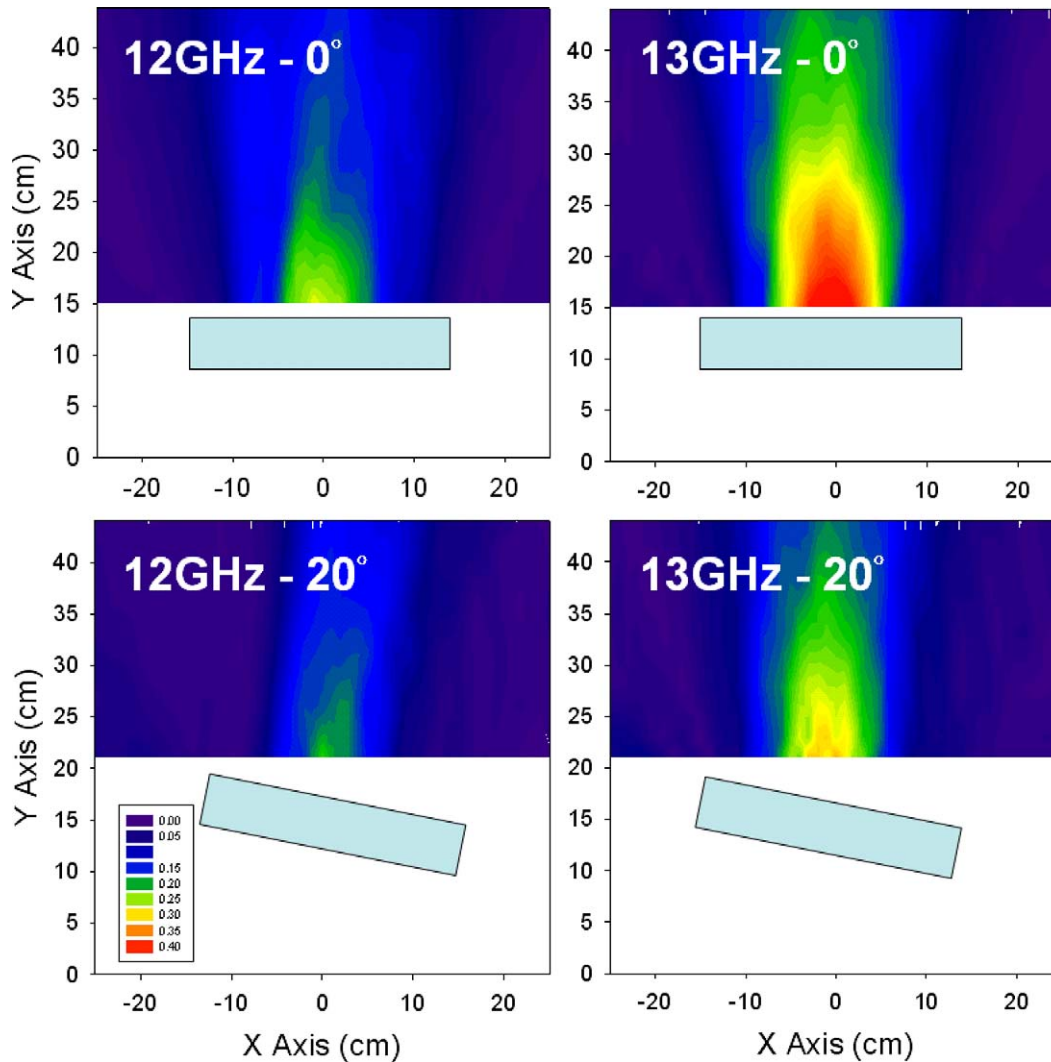


Fig. 3. The comparison of the spatial electromagnetic fields with the incident angle 0, 20 degrees respectively at frequencies 12 and 13 GHz.

angles at 0, 20 degrees respectively at frequencies of 12 and 13 GHz, and it indicates that the microwave with frequency at 12 GHz is much weaker than that at 13 GHz in intensity but with similar propagating behavior.

The spatial electromagnetic fields corresponding to different incident angles are collected in Fig. 4. It is evident that the directions of the transmitted waves are basically the same as the incident direction if the sample is rotated less than 30 degrees. When the sample revolves to a larger angle, i.e., 30 or 40 degrees, however, the outgoing waves become distinctly angled away from the incident direction. When Snell's law applied on a planar slab homogeneous medium, it predicts that the transmitted beam should keep identical direction with the incidence but shift a specific distance determined by the refractive index and the thickness of the slab medium and the angle of incidence, but our observation cannot echo this prediction. It implies that, at least with larger incident angles, it is not applicable to take such slab as a homogeneous material responding to Snell's law. After extensive and detailed examination, multiple peaks with different propagating directions wrapping up the transmitted beam are discovered. These multi-directional peaks become more appar-

ent when analyzing the angular field strength. Fig. 5(a) shows the angular distribution of the electromagnetic field in the polar chart when the sample rotates to 40 degrees. The strongest peak is found at 100 degrees, which is reflected by the interface between air and sample. Furthermore, an additional guided stray wave, which propagates along the tunnels sandwiched between two adjacent substrates, is found and identified in the direction perpendicular to normal of the sample surface. After all, the transmitted wave decomposed into several directions after passing through the sample.

4. Discussions and analysis

It is necessary to clarify the underlying mechanism of this deviation from the directive propagation. To identify the connection between the slanted transmitted wave and the multiple divergent peaks, the fundamental interference theory provides us with an intuitional explanation even the grid of the slab is in subwavelength scale. The apertures of subwavelength size make it difficult to characterize the influence of the transmitted electromagnetic wave, not to mention, the complex interlayer

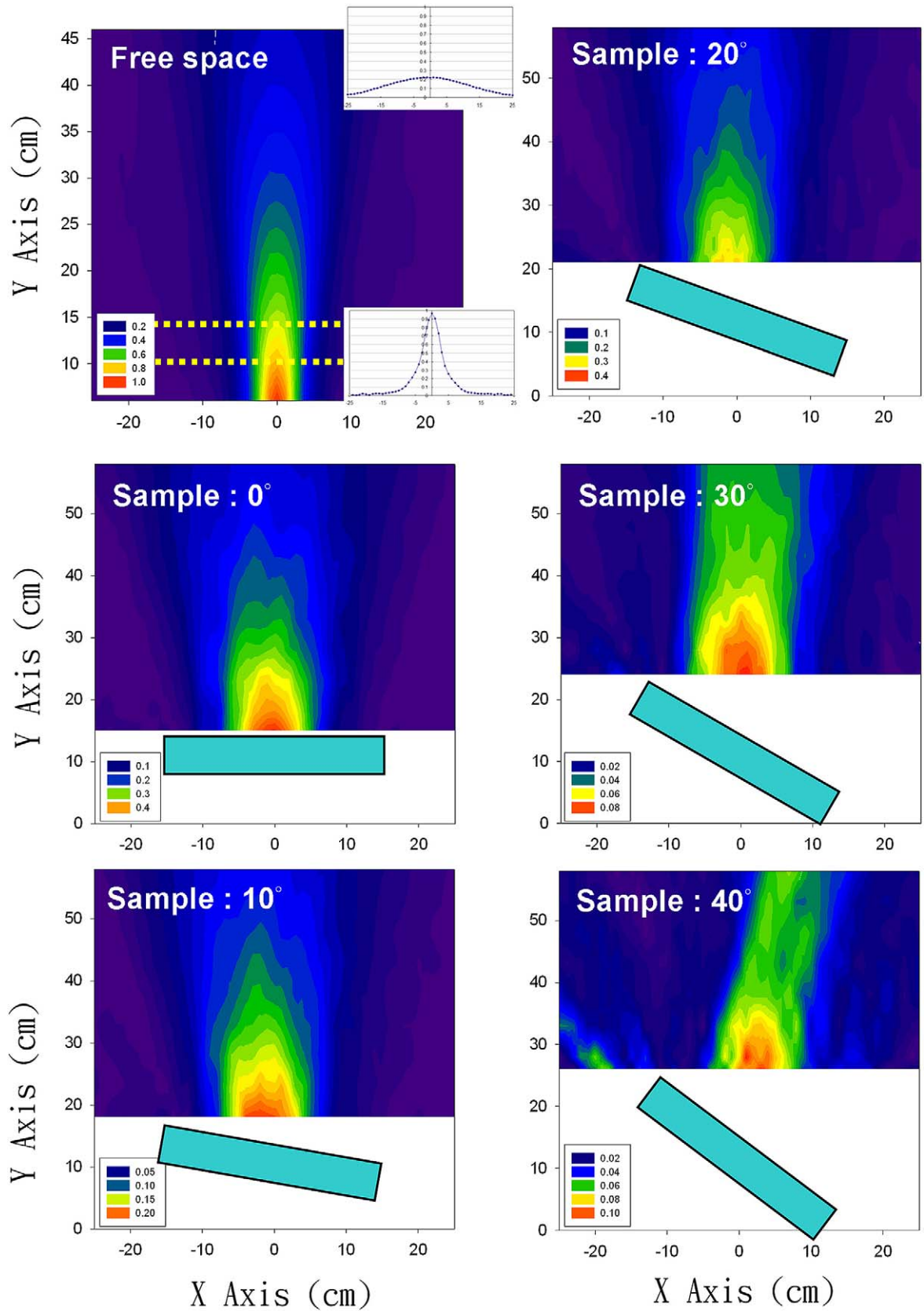


Fig. 4. The two-dimensional spatial electromagnetic field distribution diagrams. In the left top diagram the incident electro-magnetic field in free space is shown as a reference. The rest, from left top to right bottom, the EM fields measured with the sample 0, 10, 20, 30 and 40 degrees, respectively. It must be noted that the scales of these diagrams are not the same, in order to highlight the propagation direction after passing through the sample.

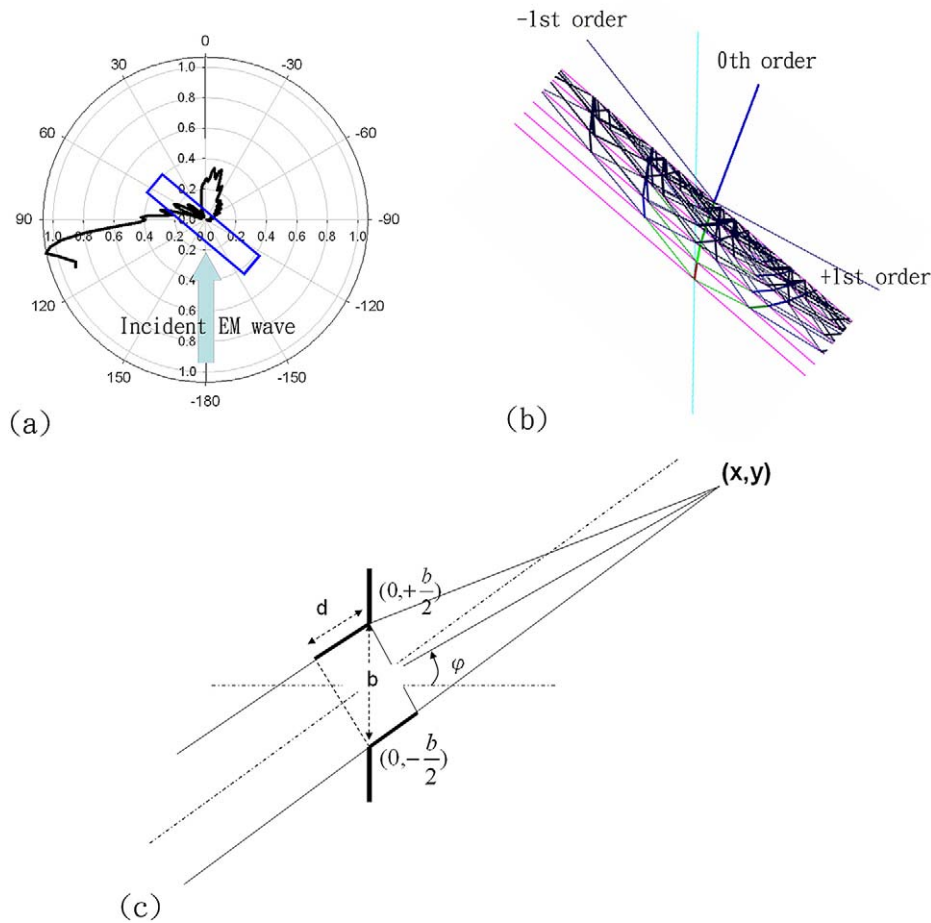


Fig. 5. (a) The angular field measurement polar chart with distance from sample rotation center to detector of 18 cm. The reflection peak appears at 100 degrees, and some energy guided by the tunnel sandwiched by the grid slabs was also found parallel to the surface of the sample. In the transmission part, several obvious peaks were examined. (b) The simulation result of the constructive interference model. +1st and -1st order rays are shown with the 0th order, except the final outgoing rays. (c) The schematic presentation of the constructive interference model.

interactions of the multiple layers. Nevertheless, the concept of phase interference still can be applied to predict the propagation direction that passes through one aperture for every single layer. The interference theory tells us that the highest energy must be analyzed at where the constructive condition is satisfied after passing through a grating. For a planar electromagnetic beam projecting on a tilted surface with grating, the transmitted energy will substantially be concentrated at a specific angle in order to satisfy the constructive condition. This angle is not necessary to be identical to the incident direction if the far-field approximation is abandoned.

Referring to Fig. 5(b), for a planar electromagnetic beam, in order to be constructively interfered with, the ray from the lower bound must make a longer transit than that from the upper bound by the amount equivalent to the initial optical path difference d in order to compensate the difference of phase before achieving aperture. Thus,

$$\sqrt{x^2 + \left(y + \frac{b}{2}\right)^2} - \sqrt{x^2 + \left(y - \frac{b}{2}\right)^2} = d + n\lambda, \quad n = \pm 1, \pm 2, \dots \quad (4)$$

Expand Eq. (4) by the second-order Taylor-series, we have

$$\tan^3 \varphi - 8 \tan \varphi + \frac{8(d + n\lambda)}{b} = 0, \quad (5)$$

where $\tan \varphi = \frac{y}{x}$.

By identifying the intersection of $y = \tan^3 \varphi - 8 \tan \varphi$ and $y = -\frac{8(d+n\lambda)}{b}$, the outgoing angle φ can be calculated. It should be emphasized that the distance of the adjacent stacking slabs is also much less than one wavelength, which implies that the near-field effect probably plays an important role in dominating the propagation behavior. By applying this scheme layer by layer, the transmitted energy for a 40-degree-revolved sample should be towards 20 degrees to the original incident direction, if our projecting electromagnetic wave is well-collimated and equal phase everywhere in the wavefront. The simulation result shown in Fig. 5(b) discloses the predicted major propagating characteristics similar to the real experimental results shown in Fig. 5(a). By examining the two-dimensional field distribution shown in Fig. 4, and the angular polar chart in Fig. 5(a), three features can be concluded.

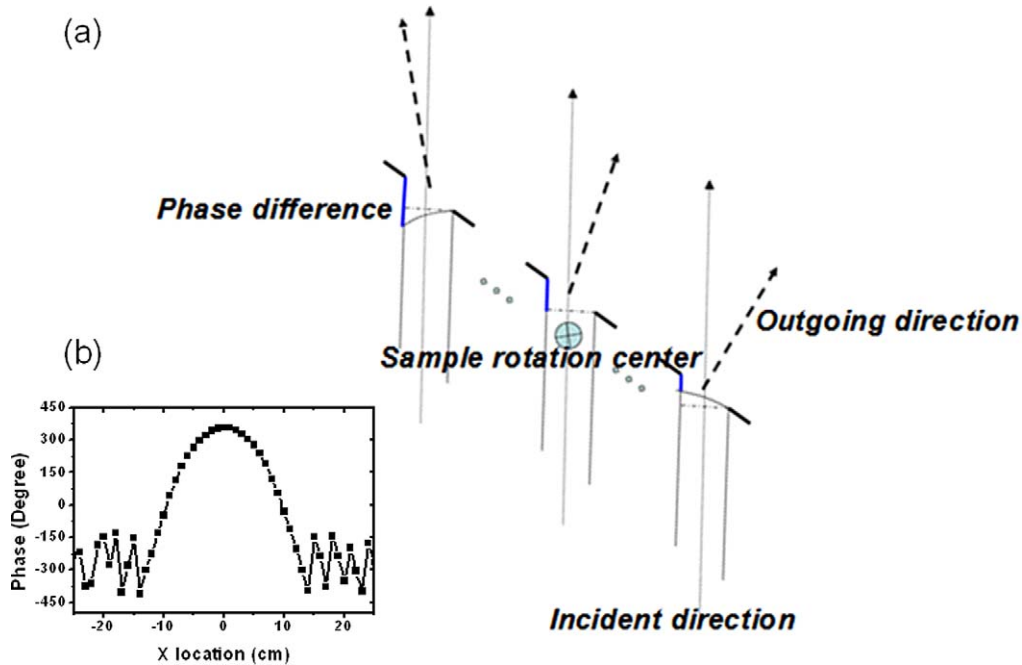


Fig. 6. (a) The schematic diagrams showing the different transmitted angles depending on the various phase difference. (b) The initial phase difference along the x -direction.

- (1) In the polar chart, it is evident that a corresponding peak appears at around 20 degrees.
- (2) In addition to the one at 20 degrees, several other peaks are also observed.
- (3) The transmitted beam is roughly 9 degrees shifting to the incident direction.

However, (2) and (3) are not consistent to what our model predicted.

To determine the possible cause of (2), the additional care for source collimation should be addressed. Our microwave source is not well collimated, even though a tube has been adopted to confine the propagation divergent angle. It broadens naturally with the propagation distance, and its intensity spreads as a Gaussian distribution, as shown in Fig. 4, as well as its phase shown in Fig. 6(b). The phase has been measured by vector network analyzer, and has found that the center of the incident electromagnetic beam leads the edge by almost 360 degrees. Due to the initial phase difference, the outgoing direction will no longer be the same as the angle predicted under the assumption of the planar electromagnetic wave. Fig. 6(a) schematically indicates the different outgoing angles due to the different initial phase lag. This might explain the multiple peaks in our measurements.

The reason for the 9 degree slant of the beam in (3) might be caused by the summation of the transmitted waves from multiple directions. However, our sample consists of six sub-wavelength identical grids, which are arrays of highly concentrated sub-wavelength apertures. The concept of constructive interference would only be able to predict the propagating direction but unable to determine the energy efficiency for each angle. This part needs further study of the electromagnetic theory and the numerical approach for clarification.

5. Conclusion

We experimentally explored the propagating behavior of a collimated microwave projecting on a metallic grid slab, and we demonstrated that the mechanism of how the incident electromagnetic wave is influenced by the subwavelength pattern is practicable. Although the embedded monopole emitter is different from the outside lens horn antenna which we used in our experiments, the angular tolerance analysis still provided us with a clear picture of the cause of the directive emission of the metallic grid slab. But a very crucial difference between our experiment and the study of other groups [18] with similar samples must be addressed, which is, our interest is to study the reason of how the incident beam propagates through a metallic grid slab but not the directive emission phenomenon. This discrepancy leads to different experimental setup and parameters. It should be emphasized that we are not willing to demonstrate the amazing directive emission in this Letter but to concentrate on the possible reason why the directive emission occurs. Furthermore, for the external incident beam, choosing the working frequency too close to the plasma frequency leads a very large part of incident energy and will be reflected from the surface of medium if the incident inclination is large. Taking working frequency in an appropriate distance from the plasma frequency improves the signal to noise ratio and eases the difficulty in examining the propagation of the outgoing beam exited from sample. It is certain that the actual behavior is much more complex than what explained by our simplified model and the detailed description of the physical mechanism remains as a matter to be discussed further. However, our works still provide a simple interpretation and a possible idea to illustrate this complicated phenomenon.

Acknowledgements

This work is partially supported by the National Science Council of Taiwan, ROC under project No. NSC92-2811-M009-019, by the Industrial Technology Research Institute, Taiwan, ROC and by the Ministry of Economics Affairs, ROC under project No. 92-EC-17-A-07-S1-0011.

References

- [1] V.G. Veselago, *Sov. Phys. Usp.* 10 (1968) 509.
- [2] D.R. Smith, W.J. Padilla, D.C. Vier, S.C. Nemat-Nasser, S. Schultz, *Phys. Rev. Lett.* 84 (2000) 4184.
- [3] D.R. Smith, D.C. Vier, N. Kroll, S. Schultz, *Appl. Phys. Lett.* 77 (2000) 2246.
- [4] R.A. Shelby, D.R. Smith, S.C. Nemat-Nasser, S. Schultz, *Appl. Phys. Lett.* 78 (2001) 489.
- [5] R.A. Shelby, D.R. Smith, S. Schultz, *Science* 292 (2001) 77.
- [6] J.B. Pendry, *Phys. Rev. Lett.* 76 (1996) 4773.
- [7] J.B. Pendry, A.J. Holden, D.J. Robbins, W.J. Stewart, *J. Phys.: Condens. Matter* 10 (1998) 4785.
- [8] J.B. Pendry, A.J. Holden, D.J. Robbins, W.J. Stewart, *IEEE Trans. Microwave Theory Tech.* 47 (1999) 2075.
- [9] A. Lakhtakia, *Int. J. Electron. Commun.* 58 (2004) 229.
- [10] A. Lakhtakia, *Opt. Express* 11 (2003) 716.
- [11] J.Q. Shen, *Phys. Lett. A* 344 (2005) 144.
- [12] J.Q. Shen, *Ann. Phys. (Leipzig)* 13 (2004) 335.
- [13] J.B. Pendry, *Phys. Rev. Lett.* 85 (2000) 3966.
- [14] J.S. Lih, Y.S. Wang, M.C. Lu, Y.C. Huang, K.H. Chen, J.L. Chern, L.E. Li, *Europhys. Lett.*, in press.
- [15] Y.C. Huang, Y.J. Hsu, J.S. Lih, J.L. Chern, *Jpn. J. Appl. Phys. Lett.* 43 (2004) L190; Y.J. Hsu, Y.C. Huang, J.S. Lih, J.L. Chern, *J. Appl. Phys.* 96 (2004) 1979.
- [16] Y.J. Hsu, J.L. Chern, *Jpn. J. Appl. Phys. Lett.* 43 (2004) L669.
- [17] P.F. Loschialpo, D.W. Forester, D.L. Smith, F.J. Rachford, *Phys. Rev. E* 70 (2004) 036605.
- [18] S. Enoch, G. Tayeb, P. Sabouroux, N. Guerin, P. Vicent, *Phys. Rev. Lett.* 89 (2002) 2139.
- [19] D. Felbacq, G. Bouchitte, *Waves Random Media* 7 (1997) 245.
- [20] G. Guida, D. Maystre, G. Tayeb, P. Vincent, *J. Opt. Soc. Am. B* 15 (1998) 2308.